



## Article

# New Machine Learning Approach for the Optimization of Nano-Hybrid Formulations

Raquel de M. Barbosa<sup>1,2,\*</sup>, Cleanne C. Lima<sup>1</sup>, Fabio F. de Oliveira<sup>3</sup>, Gabriel B. M. Câmara<sup>1,3</sup>, César Viseras<sup>2</sup>, Tulio F. A. de Lima e Moura<sup>1</sup>, Eliana B. Souto<sup>4,5,\*</sup>, Patricia Severino<sup>6,7</sup>, Fernanda N. Raffin<sup>1</sup> and Marcelo A. C. Fernandes<sup>3,8</sup>

- <sup>1</sup> Laboratory of Drug Development, Department of Pharmacy, Federal University of Rio Grande do Norte, Natal 59078-970, Brazil; cleanne@ufrn.edu.br (C.C.L.); gmottaz@gmail.com (G.B.M.C.); moura@ufrnet.br (T.F.A.d.L.e.M.); feraffin@ufrnet.br (F.N.R.)
  - <sup>2</sup> Department of Pharmacy and Pharmaceutical Technology, Faculty of Pharmacy, Campus de Cartuja s/n, University of Granada, 18071 Granada, Spain; cviseras@ugr.es
  - <sup>3</sup> Laboratory of Machine Learning and Intelligent Instrumentation, IMD/nPITI, Federal University of Rio Grande do Norte, Natal 59078-970, Brazil; fabio.veritate@gmail.com (F.F.d.O.); mfernandes@dca.ufrn.br (M.A.C.F.)
  - <sup>4</sup> Department of Pharmaceutical Technology, Faculty of Pharmacy, University of Porto, Rua de Jorge Viterbo Ferreira, No. 228, 4050-313 Porto, Portugal
  - <sup>5</sup> REQUIMTE/UCIBIO, Faculty of Pharmacy, University of Porto, Rua de Jorge Viterbo Ferreira, No. 228, 4050-313 Porto, Portugal
  - <sup>6</sup> Laboratory of Nanotechnology and Nanomedicine (LNMED), Institute of Technology and Research (ITP), Av. Murilo Dantas 300, Aracaju 49010-390, Brazil; patricia\_severino@itp.org.br
  - <sup>7</sup> Industrial Biotechnology Program, University of Tiradentes (UNIT), Av. Murilo Dantas 300, Aracaju 49032-490, Brazil
  - <sup>8</sup> Department of Computer Engineering and Automation, Federal University of Rio Grande do Norte, Natal 59078-970, Brazil
- \* Correspondence: rbarbosa@ugr.es (R.d.M.B.); ebsouto@ff.up.pt (E.B.S.)



**Citation:** Barbosa, R.d.M.; Lima, C.C.; Oliveira, F.F.d.; Câmara, G.B.M.; Viseras, C.; Moura, T.F.A.d.L.e.; Souto, E.B.; Severino, P.; Raffin, F.N.; Fernandes, M.A.C. New Machine Learning Approach for the Optimization of Nano-Hybrid Formulations. *Nanomanufacturing* **2022**, *2*, 82–97. <https://doi.org/10.3390/nanomanufacturing2030007>

Academic Editor: Andres Castellanos-Gomez

Received: 21 June 2022

Accepted: 15 July 2022

Published: 18 July 2022

**Publisher's Note:** MDPI stays neutral with regard to jurisdictional claims in published maps and institutional affiliations.



**Copyright:** © 2022 by the authors. Licensee MDPI, Basel, Switzerland. This article is an open access article distributed under the terms and conditions of the Creative Commons Attribution (CC BY) license (<https://creativecommons.org/licenses/by/4.0/>).

**Abstract:** Nano-hybrid systems are products of interactions between organic and inorganic materials designed and planned to develop drug delivery platforms that can be self-assembled. Poloxamine, commercially available as Tetronic<sup>®</sup>, is formed by blocks of copolymers consisting of poly (ethylene oxide) (PEO) and poly (propylene oxide) (PPO) units arranged in a four-armed star shape. Structurally, Tetronics are similar to Pluronic<sup>®</sup>, with an additional feature as they are also pH-dependent due to their central ethylenediamine unit. Laponite is a synthetic clay arranged in the form of discs with a diameter of approximately 25 nm and a thickness of 1 nm. Both compounds are biocompatible and considered as candidates for the formation of carrier systems. The objective is to explore associations between a Tetronic (T1304) and LAP (Laponite) at concentrations of 1–20% (*w/w*) and 0–3% (*w/w*), respectively. Response surface methodology (RSM) and two types of machine learning (multilayer perceptron (MLP) and support vector machine (SVM)) were used to evaluate the physical behavior of the systems and the  $\beta$ -Lapachone ( $\beta$ -Lap) solubility in the systems.  $\beta$ -Lap (model drug with low solubility in water) has antiviral, antiparasitic, antitumor, and anti-inflammatory properties. The results show an adequate machine learning approach to predict the physical behavior of nanocarrier systems with and without the presence of LAP. Additionally, the analysis performed with SVM showed better results ( $R^2 > 0.97$ ) in terms of data adjustment in the evaluation of  $\beta$ -Lap solubility. Furthermore, this work presents a new methodology for classifying phase behavior using ML. The new methodology allows the creation of a phase behavior surface for different concentrations of T1304 and LAP at different pHs and temperatures. The machine learning strategies used were excellent in assisting in the optimized development of new nano-hybrid platforms.

**Keywords:** clay; polyamines; response surface methodology; machine learning; support vector machine; multilayer perceptron; thermo responsive gels; pH-responsive gels

## 1. Introduction

Polymer micelles have been studied as a viable alternative for gene delivery systems, drugs, or contrast agents [1–7]. Polymeric therapy is arguably one of the most successful alternatives when dealing with first-generation nanotechnology carriers. Among them, polymeric micellar systems stand out, which have great potential for success [8]. Micellar systems are formed by blocks of amphiphilic copolymers and have been used in treating, diagnosing, and monitoring an illness. These theragnostic systems have attracted much attention in the medical, biological, and pharmaceutical fields [9]. Polyamines, commercially available as Tetronic<sup>®</sup>, are formed by blocks of copolymers consisting of poly (ethylene oxide) (PEO) and poly (propylene oxide) (PPO) units arranged in a four-armed star shape with different hydrophilic-lipophilic balance (HBL), and molecular weight [10,11], being very attractive as drug delivery systems due to the capacity to form nanometric structures as micelles or worm-like micelles, for example, [12–14]. Structurally, Tetronics are similar to Pluronic<sup>®</sup> [15–17]. PEO-PPO-PEO copolymer block micelles (Pluronic) incorporating doxorubicin (SP1049C) are used in clinical studies as anticancer agents [18].

Recent studies have shown that micelles formed by Tetronics have the same favorable attributes as Pluronic, however, with an additional benefit, as they are pH-dependent due to their central ethylenediamine unit [15,19]. The influence of pH on its structural organization provides a relevant and favorable feature to the delivery system of substances to a specific site, such as the delivery of antineoplastic in tumor tissue; this is due to the increase in glucose that raises (abnormally) the concentration of lactic acid by malignant cells (Warburg effect) [20]. Furthermore, according to [21], there is evidence that Tetronics can also inhibit efflux pumps in a similar way to Pluronic, which would be another great advantage for neoplasm therapy.

It is known that the combination of Laponite (LAP,  $\text{Na}^+_{0.7}[(\text{Si}_8\text{Mg}_5.5\text{Li}_{0.3})\text{O}_{20}(\text{OH})_4]^{-0.7}$ ), discs of synthetic smectite clays with a diameter of approximately 25 nm and a thickness of 1 nm, with Pluronic block copolymers leads to the formation of hydrogels [17,18]. LAP has negative-charge surfaces with pH-dependent edges [22–24].

Nano-hybrid systems were presented as an attractive platform for drug delivery. These systems combine organic and inorganic materials in self-assembled structures [25]. Recent research has also shown that compounds formed by polyethylene oxide (PEO) and PEO/chitosan associated with LAP promote cell adhesion, proliferation, and differentiation [26]. Furthermore, according to [27], complexes formed by Laponite and alginate were able to promote the sustained release of doxorubicin, which was more significant with the reduction in pH.

Several studies have been published focusing on composite formulations with Tetronic co-polymers associated or not with laponite nanoparticles. This association can modify the transition of sol–gel phases of nanocomposites formed and provide a sustained release of dependence temperature and/or pH [28–30]. For these reasons, they can be a desirable platform for multifunctional, innovative therapy with excellent prospects for cancer treatment.

Beta-lapachone ( $\beta$ -Lap) is a naphthoquinone synthesized from Lapachol. Lapachol is a phenolic compound extracted from trees of the Bignoniaceae family, *Tabebuia*, widely found in northern and northeastern Brazil. A high quantity of research indicates  $\beta$ -Lap as a drug with antiviral, antiparasitic, antitumor, and anti-inflammatory activities [31,32]. However, its low water solubility ( $0.038 \text{ mg} \cdot \text{mL}^{-1}$ ) provides serious bioavailability problems [33,34], making its use unfeasible.

The different stages of developing new pharmaceutical products, in general, demand a lot of time and money; in carrier systems, it is no different since there is a great possibility of organic and inorganic compounds that can be used to prepare nanocomposites. Studies reporting the optimized design of experiments are classic approaches and are widely used nowadays. Optimizing the parameters used during development allows for evaluating the impact of each variable (input data) on the target (output data). The response surface methodology (RSM) technique created in 1951 by Box and Wilson [35] is widely used in the

chemical and pharmaceutical industry to optimize experimental procedures when seeking to reduce the number of experiments. The RSM searches through mathematical models for possible impacts of factors related to a process and points out an ideal working region with answers individually and cumulatively in response to a system [36].

Artificial intelligence (AI) based on machine learning (ML) has been increasingly used in different areas of knowledge. For example, ML techniques and algorithms allow a new analysis alternative and have accelerated discoveries of materials and formulations in the pharmaceutical field [37–47].

ML techniques, such as the support vector machine (SVM), and those based on artificial neural networks (ANNs), such as multilayer perceptron (MLP), can find input and output relationships for complex nonlinear systems associated with multiple variables. From a set of experimental data, ML techniques (MLP and SVM) can learn regression and classification models for any system [42]. The MLP technique has been successfully used in the literature to obtain regression models. However, this technique requires a lot of experimental data for training and validation [42], which in some cases can be prohibitive. On the other hand, SVM works well with a small dataset, generating very reliable response surfaces and classification models [47–51].

All aspects of this study are considered relevant to the potential development of Tetronic-based systems. The objective is, therefore, to use RSM and ML (SVM and MLP) techniques [47–49] to optimize different T1304 and LAP concentrations to find the most efficient formulations to solubilize  $\beta$ -Lap. In addition, this work presents a novel methodology based on phase behavior classification using ML. This novel methodology enables the creation of a phase behavior surface for different concentrations of T1304 and LAP at different pHs (natural pH, pH 2.0, pH 5.5, and pH 7.4) and with a temperature ramp between 25–70 °C.

Finally, our results can promote important information to rapidly advance the designing of an attractive platform for multifunctional treatment, based on its low cost, combined with good biological activity, the favorable characteristics of micellar systems as carriers of drugs and contrast agents, and the wealth of data generated with the Pluronic<sup>®</sup> micelles.

## 2. Materials and Methods

### 2.1. Materials

Poloxamine with 21 and 27 PEO and PPO units, respectively (Tetronic 1304 with MM 10,500 Dalton and HBL: 12–18), was donated by the manufacturer BASF Corporation (Ludwigshafen, Germany). BYK Additives & Instruments (Wesel, Germany) kindly provided Laponite RD, a synthetic clay. The  $\beta$ -Lap compound was obtained from the laboratory of Professor Celson Camara of the Federal Rural University of Pernambuco (UFRPE, Recife, Brazil). This was achieved by a simple process of acid cyclization of Lapachol under acidic conditions and low temperatures. The other reagents used in this work, but not described in this section, are available and considered as analytical grade.

### 2.2. Methods

#### 2.2.1. Preparation of the Nanocarriers

All nanocarrier systems (unique compound and hybrid) were similarly prepared. The mixtures of poloxamine (T1304) with or without LAP were kept in a bath sonicator for approximately 20 min at room temperature, then held under magnetic stirring for 24 h. The used concentrations of T1304 ranged over 1–20%, *w/w* with and without the presence of 1.5 or 3% *w/w* of LAP. Additionally, pH influence was studied at pH 2.0, pH 5.5, pH 7.0, and natural pH (~8.2 for nanocarriers in the absence of LAP and ~10 in the presence of LAP). All pHs were adjusted, with HCL at 1 mol.L<sup>-1</sup>) [30].

### 2.2.2. Characterization of the Nanocarriers Physical Behavior of Systems

The systems were evaluated for physical behavior by visual observation. In addition, the samples were all subjected to a stepwise temperature increase of 20 to 80 °C (increments of 5 °C, 10 min intervals between each sample stabilization). The experiments were conducted with samples in triplicate and the parameters used for data analysis and classification are described in Table 1.

**Table 1.** Parameters used for data analysis and classification of systems.

Physical Behavior	Parameters Used
Liquid	Clear liquid and unable to maintain its weight if the bottle is inverted.
Viscous liquid	Thicker liquid with slower sample flow. Additionally, unable to maintain its weight if the bottle is inverted.
Gel	Classified as transparent dispersions in the form of a gel and capable of maintaining their weight if the vial is inverted; however, if subjected to vigorous agitation for 10 s, they come off.
Strong gel	Classified as clear dispersions in the form of a firm gel, capable of maintaining their weight against gravity in an inverted flask, and if subjected to vigorous shaking for 10 s, they do not come off.

#### Phase Behavior Experimental Design using Machine Learning

The ML used to classify the phase behavior was characterized by a committee composed of four SVMs, as presented in Figure 1. The ML was trained to classify four-phase behavior represented by liquid, viscous liquid, gel, and strong gel. Each  $k$ th SVM ( $SVM_k$ ) inside the committee was a binary classifier, and it was responsible for one of each class, i.e., liquid ( $SVM_1$ ), viscous liquid ( $SVM_2$ ), gel ( $SVM_3$ ), and strong gel ( $SVM_4$ ). The inputs associated with each  $k$ th SVM were associated with the proportion of T1304 ( $x_1$ ), the proportion of LAP ( $x_2$ ), and the temperature ( $x_3$ ) in Celsius degrees.

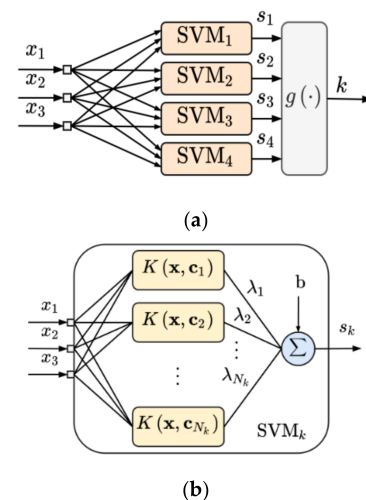


**Figure 1.** The ML approach used to classify the phase behavior. (a) The SVM committee architecture composed of four SVMs. (b) The  $k$ th SVM of the SVM committee. Each SVM is associated with one of the four classes: liquid ( $k = 1$ ), viscous liquid ( $k = 2$ ), gel ( $k = 3$ ), and strong gel ( $k = 4$ ).

The Gaussian kernel with the sequential minimal optimization (SMO) algorithm were used for each  $k$ th SVM. The Gaussian kernel can be represented as

$$K(x, c_i) = e^{-\frac{1}{2\sigma}x - c_i^2} \quad (1)$$

where  $x = [x_1, x_2, x_3]$  is the vector input and  $c_i$  is the center of the  $i$ th kernel, also called support vectors [42,47,48]. The output of each  $k$ th SVM was combined to generate the unique output that represents one of the  $k$ th classes. The proposed ML output is characterized by

$$k = g\left(\text{index}(\max\{s_1, s_2, s_3, s_4\})\right) \quad (2)$$

where the variables  $\{s_1, s_2, s_3, s_4\}$  represent the output of each  $k$ th SVM. The training and validation used  $n$ -fold cross-validation with  $n = 5$ .

### $\beta$ -Lap Solubility in Nanosystems: Factorial and Machine Learning Analyses

A total of 5 mg of  $\beta$ -Lap was added to each 1 g sample (single or hybrid systems). Thus, in excess of the drug, all vials were kept under continuous agitation for ten days, without interruption, using the Blood Homogenizer and Solutions Model AP 22 (Phoenix-Luferco, Araraquara, Brazil). Subsequently, the systems were centrifuged (14,000 rpm for 15 min at 20 °C), and the supernatant was evaluated by UV-Vis spectrophotometry at 257 nm. The calibration curve comprised values between 2–10  $\mu\text{g mL}^{-1}$  of  $\beta$ -Lap solubilized in an ethanolic solution (1:1). The drug was quantified using the linear least squares rule by the equation  $y = 0.1123x + 0.0041$ ,  $R^2 = 0.9998$  [33].

### Design of Experiments by Central Composite Design

The central composite design (CCD) factorial design was used to generate the results associated with  $\beta$ -Lap solubility. The factorial design was formulated with 32 assays (two factors and three levels) (see Table 2). The surface's coefficient of determination ( $R^2$ ) was obtained using the computational tool MATLAB 2020 (License 650662, Mathworks, Natick, MA, USA). The final expression found for the solubility surface is characterized as:

$$\beta\text{-Lap}_{(\mu\text{g.mL}^{-1})} = \beta_0 + \beta_1x_1 + \beta_2x_2 + \beta_{11}x_1^2 + \beta_{22}x_2^2 + \beta_{12}x_1x_2 \quad (3)$$

where the variables  $x_1$  (T1304 concentration) and  $x_2$  (LAP concentration) are the independent variables. The  $\beta_0, \beta_1, \beta_2, \beta_{11}, \beta_{22}$ , and  $\beta_{12}$  are linear and quadratic coefficients.

**Table 2.** Factorial design formulated with 32 assays. Two factors and three levels, i.e.,  $3^2$ .

Assays	T1304 ( $x_1$ )		LAP ( $x_2$ )		$\beta$ -Lap <sup>1</sup>
	Coded Level	% (w/w)	Coded Level	% (w/w)	$\mu\text{g/mL}$
1	−1	1	−1	0.0	0.1206
2	−1	1	0	1.5	0.2600
3	−1	1	+1	3.0	0.4264
4	0	10	−1	0.0	0.4281
5	0	10	+1	3.0	0.5103
6	+1	20	−1	0.0	1.0211
7	+1	20	0	1.5	1.6062
8	+1	20	+1	3.0	0.9988
9	0	10	0	1.5	0.7875
10	0	10	0	1.5	0.8010
11	0	10	0	1.5	0.7780
12	0	10	0	1.5	0.7650

<sup>1</sup>  $\beta$ -Lap in the nanocarriers: from solubility studies.

### Design of Experiments by Machine Learning (MLP and SVM)

This experiment used two ML techniques to determine a surface response. The methods were the MLP (see Figure 2a) and SVM (see Figure 2b). Analogous to the RSM approach based on CCD factorial design (see Equation (3)), the ML techniques used as inputs the T1304 ( $x_1$ ) and LAP ( $x_2$ ) concentrations.

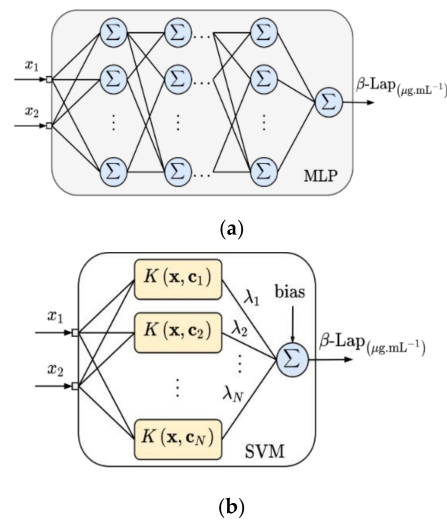


**Figure 2.** The ML techniques implemented to determine a surface response of  $\beta$ -Lap solubility. (a) The MLP architecture. (b) The SVM architecture.

The ML based on MLP works with two hidden layers (with 16 neurons each), sigmoid activation function in all hidden neurons, and linear function in the output neuron. The training strategy was based on the Levenberg–Marquardt backpropagation algorithm [42,47,48]. The surface response based on MLP is characterized as:

$$\beta - Lap = \sum_{q=1}^{16} w_{1q}^3 \varnothing \left( \sum_{m=1}^{16} w_{qm}^2 f(w_{m1}^1 x_1 + w_{m2}^1 x_2 + w_{m0}^1) + w_{q0}^2 \right) + w_{10}^3 \quad (4)$$

where  $f(\cdot)$  and  $\varnothing(\cdot)$  are the sigmoid and linear activation function, respectively. The variable the  $w_{ij}^k$  is  $j$ th weight associated with the  $i$ th neuron in the  $k$ th layer. The surface response based on SVM is expressed by

$$\beta - Lap = \sum_{i=1}^N \lambda_i K(\mathbf{x}, \mathbf{c}_i) + bias \quad (5)$$

where  $\lambda_i$  is the  $i$ th gain. The MLP and SVM techniques were trained with 90% and validated with 10% of the samples.

The MLP and SVM models were created with the same data used in the RSM approach (see Table 2) plus additional values presented in Table 3. The assays 1–12 (see Table 2) and 12–18 (see Table 3) were used in the training step and assays 19–21 in Table 3 were used in the validation step.

**Table 3.** Experimental design of the values that were included and used to improve training and validation of ML (SVM and MLP). Assays (1–12) shown in Table 2 were also used in these experiments.

Assays	T1304 ( $x_1$ )	LAP ( $x_2$ )	$\beta$ -Lap <sup>1</sup>
	Coded Level	% ( $w/w$ )	Coded Level
13	5	0.0	0.2092
14	5	1.5	0.4792
15	5	3.0	0.3617
16	15	0.0	0.3639
17	15	1.5	1.1375
18	15	3.0	0.8039
19	8	0.0	0.4618
20	20	1.0	0.1397
21	20	2.0	1.2785

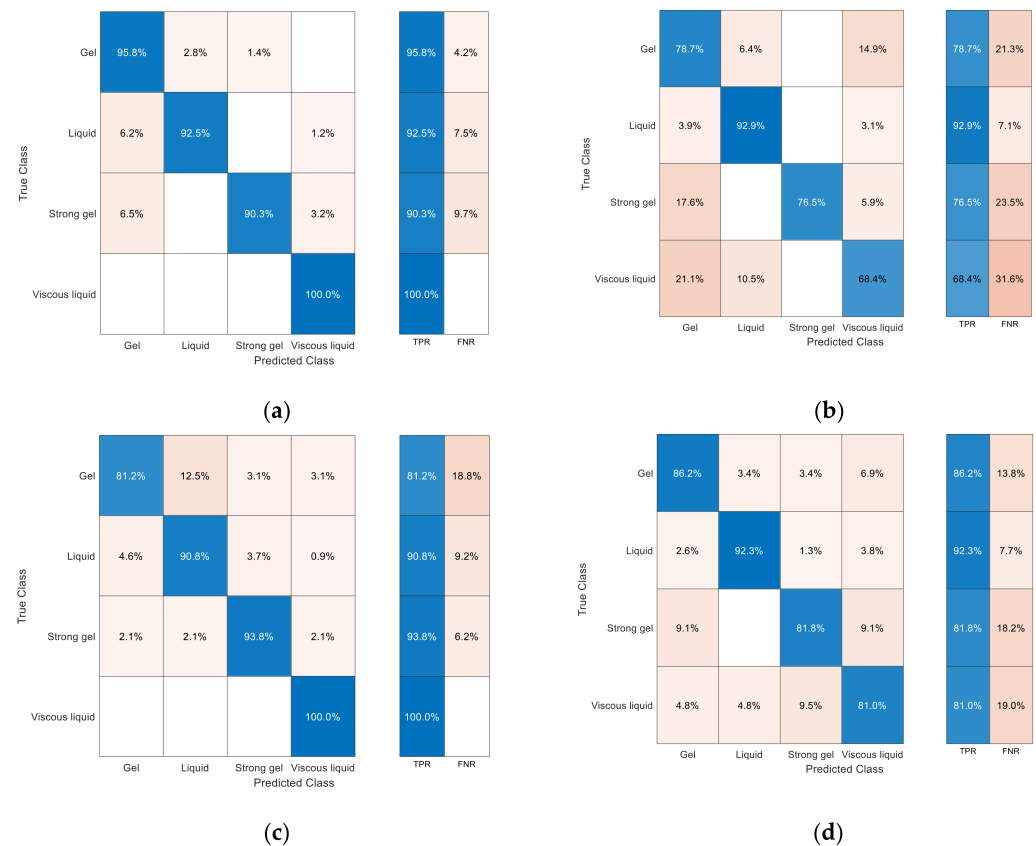
<sup>1</sup>  $\beta$ -Lap in the nanocarriers: from solubility studies.

### 3. Results and discussion

#### 3.1. Physical Behavior Analysis

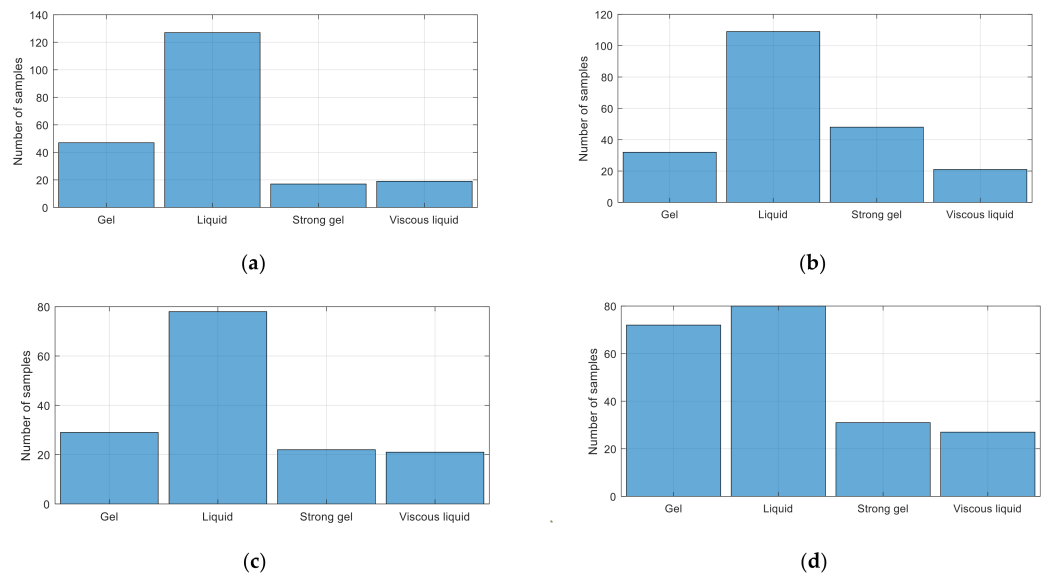
The ML technique based on SVM was applied to classify the physicists of the formulations under different temperature and pH conditions since they are thermo- and pH-responsive substances. The analysis enabled the classification and prediction of different physical states (four classes, see Table 3).

Figure 3a–d show the confusion matrix data and physical behavior for different concentrations of T1304 with or without LAP. The results were obtained for pH 2.0, 5.5, 7.4, and natural pH over a wide temperature range using SVM models. The SVM models for the physical behavior classification used  $N_1 = 58$ ,  $N_2 = 50$ ,  $N_3 = 7$ , and  $N_4 = 25$  kernels on SVM<sub>1</sub>, SVM<sub>2</sub>, SVM<sub>3</sub>, and SVM<sub>4</sub>, respectively. The confusion matrix data of SVM depicted an accuracy between 90 and 100% (values displayed diagonally in blue boxes).



**Figure 3.** SVM confusion matrix data for physical behaviour with different T1304 concentrations with or without LAP at (a) pH 2.0, (b) pH 5.5, (c) pH 7.4, and (d) natural pH, over a temperature range between 25 to 70 °C. Note: TPR is true positive rate and FNR is false negative rate.

The sensitivity of the applied model (true positive rate or TPR) revealed values between 68.4 and 100% and specificity (false negative rate or FNR) between 0 and 31.6%, varying according to the sample dataset. Samples submitted to pH 5.5 conditions showed the lowest percentages of TPR and FNR. It is important to mention that a cross-validation strategy with five folds was used, where 90% of the data were destined for training and 10% for validation. Despite the non-balancing of the data in all conditions used (Figure 4), only for the pH 5.5 condition the classification and prediction results were not as satisfactory as the other conditions evaluated. Another important aspect to highlight is that, despite the number of samples in the liquid condition, no trend was observed for this class. The accuracies led us to choose the SVM model for the classification and prediction of data.



**Figure 4.** Histogram of the samples prepared with varying concentrations of T1304 with or without LAP used for SVM training and validation. The samples were labeled based on their physical state when subjected to conditions of (a) pH 2.0, (b) pH 5.5, (c) pH 7.4, and (d) natural pH, over a temperature range between 25 to 70 °C.

Based on Figure 5, samples with T1304 (1–20%, *w/w*) (without LAP) were classified as liquid samples in all concentrations, and temperature ranges were studied. These samples had a phase transition behavior (sol–gel) only above 75 °C. The positive influence of LAP as an ingredient in the formulation can be seen in Figure 4b,c. In this case, it was verified that the LAP can modify the physical behavior of the samples for different temperatures. Based on the results presented in Figure 4b,c, the LAP at one concentration generates samples with the four different physical states for different temperatures. This result shows that they are good candidates for future studies on developing drug delivery nanocarriers.

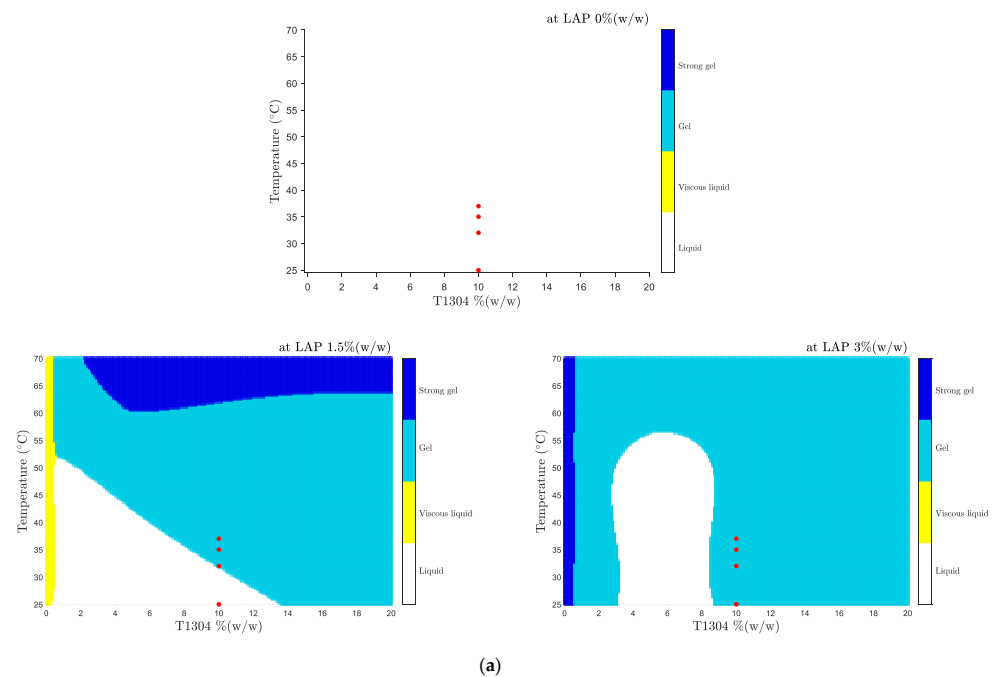


**Figure 5.** Cont.

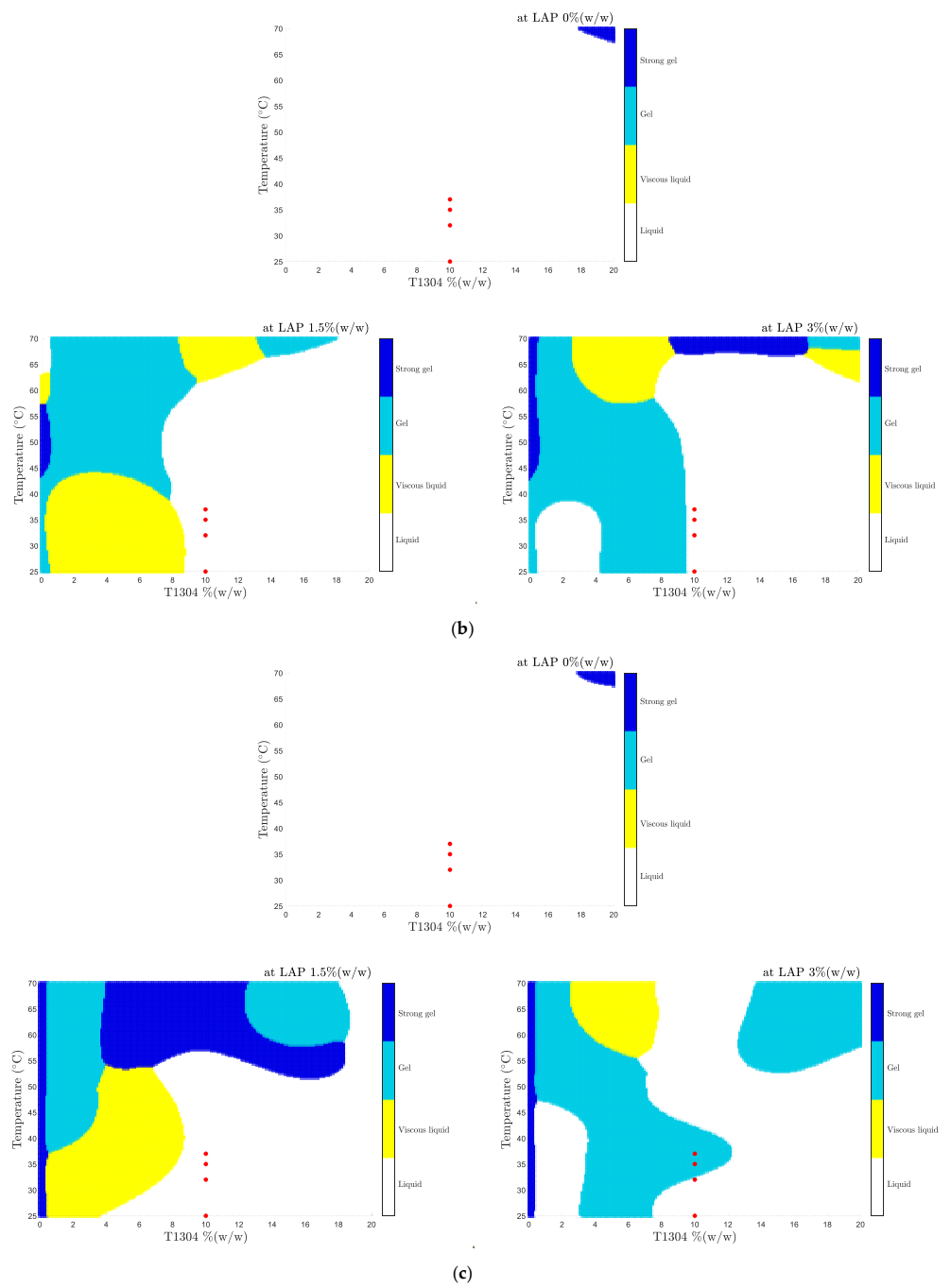
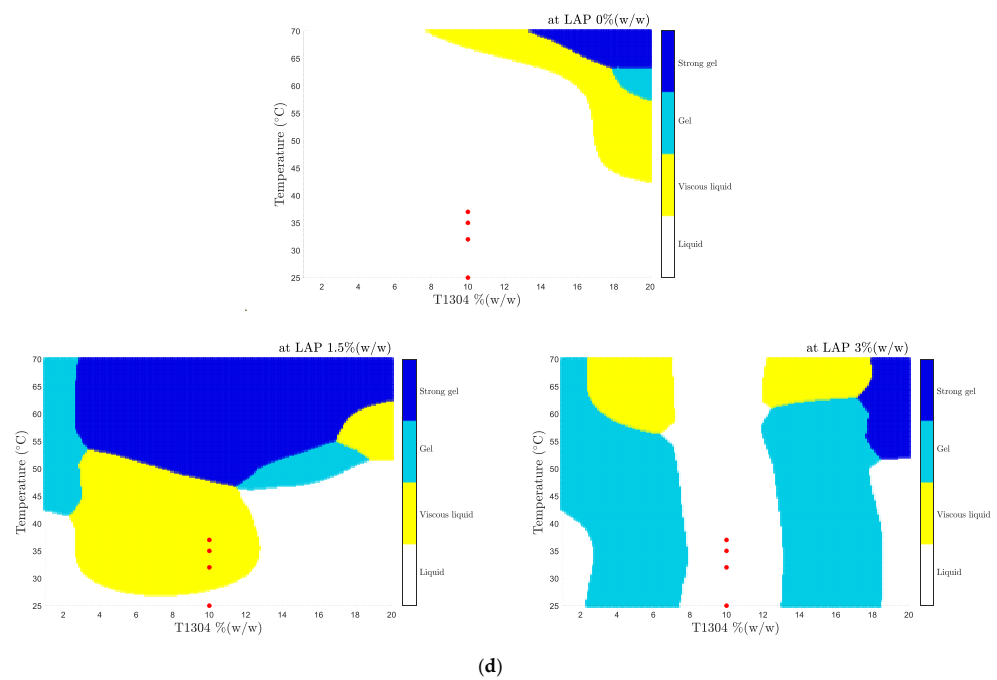
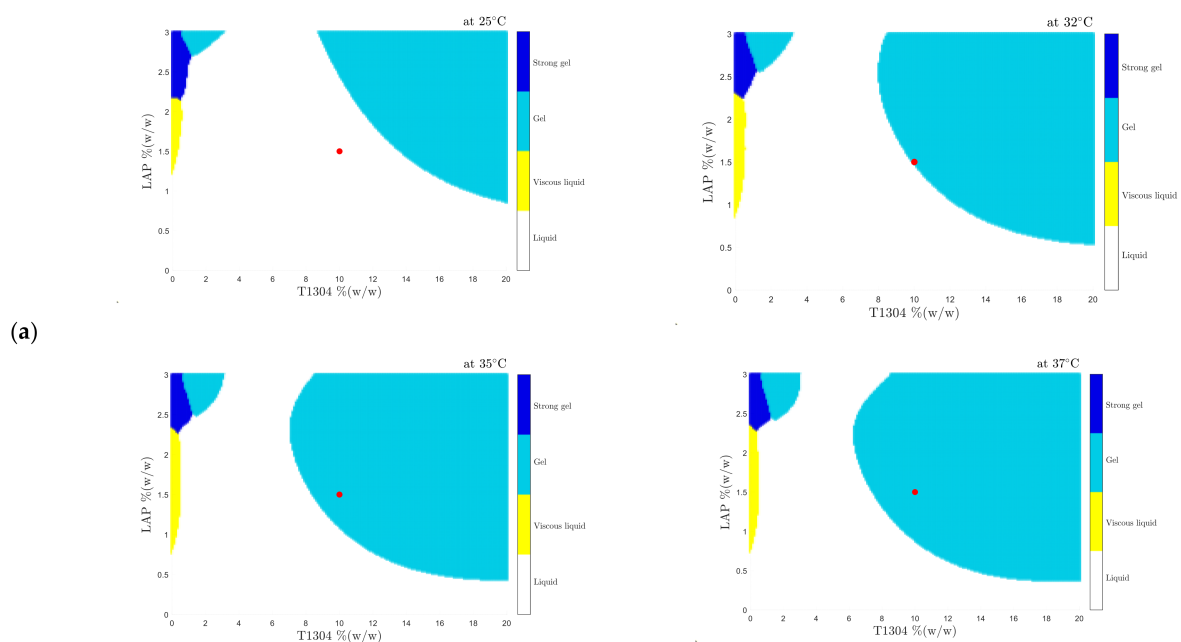


Figure 5. Cont.



**Figure 5.** Graphic representation of the SVM classification of the phase behavior for different concentrations of T1304 and LAP at different pHs ((a) natural pH, (b) pH 2.0, (c) pH 5.5, and (d) pH 7.4) and with a temperature ramp between 25–70 °C. In red, the sample with 10% (*w/w*) of T1304 (with and without LAP) is observed at 25 °C and body temperature (32 °C, 34 °C, and 37 °C).

Unlike Figure 5, Figure 6 presents the phase behavior for the entire concentration domain of T1304 and LAP studied at 25 °C, 32 °C, 35 °C, and 37 °C. In this case, the results show that nano-hybrid systems have a transition phase from sol–gel to body temperatures (32 °C, 35 °C, and 37 °C). The determination of these properties is very interesting because, depending on the route of administration, the prior knowledge of these characteristics makes possible the optimized planning for developing promising formulations, the best bioavailability, and drug release.



**Figure 6.** Cont.

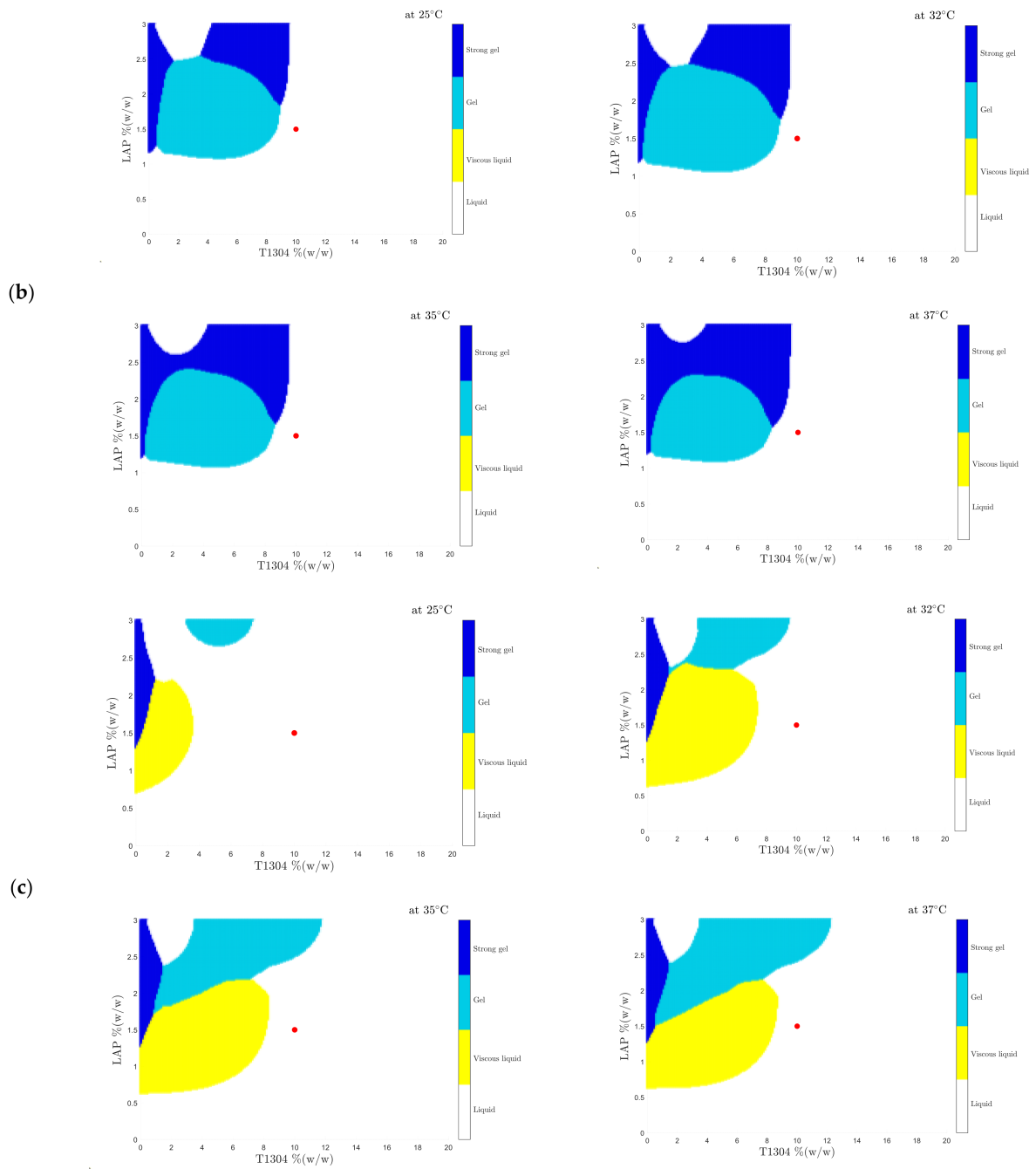
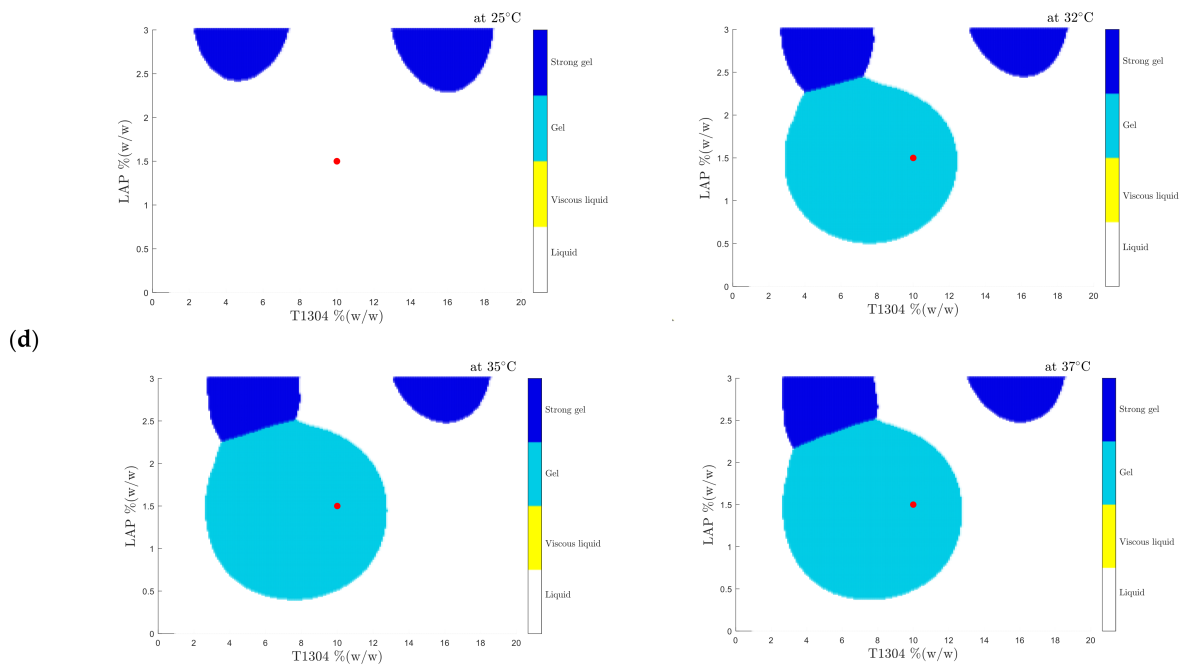


Figure 6. Cont.



**Figure 6.** Classification of phase behavior diagrams of systems at different temperatures and pHs. The red dots highlight that minor temperature changes generate changes in the physical state of the samples, such as 10% T1304 and 1.50% LAP. Red dots represent 10% T1304 concentration with 1.5% LAP. Temperatures: 25 °C representing ambient temperature and body fluid temperatures (32 °C, 35 °C, and 37 °C). pHs studied: (a) natural pH, (b) pH 2.0, (c) pH 5.5, and (d) pH 7.4 (body fluids).

3.2. *β-Lap Solubility Analysis*

Figure 7a–c present the surface response concerning the influence of the concentrations of T1304 and LAP on the solubility of *β*-Lap for the RSM, MLP, and SVM methods, respectively.

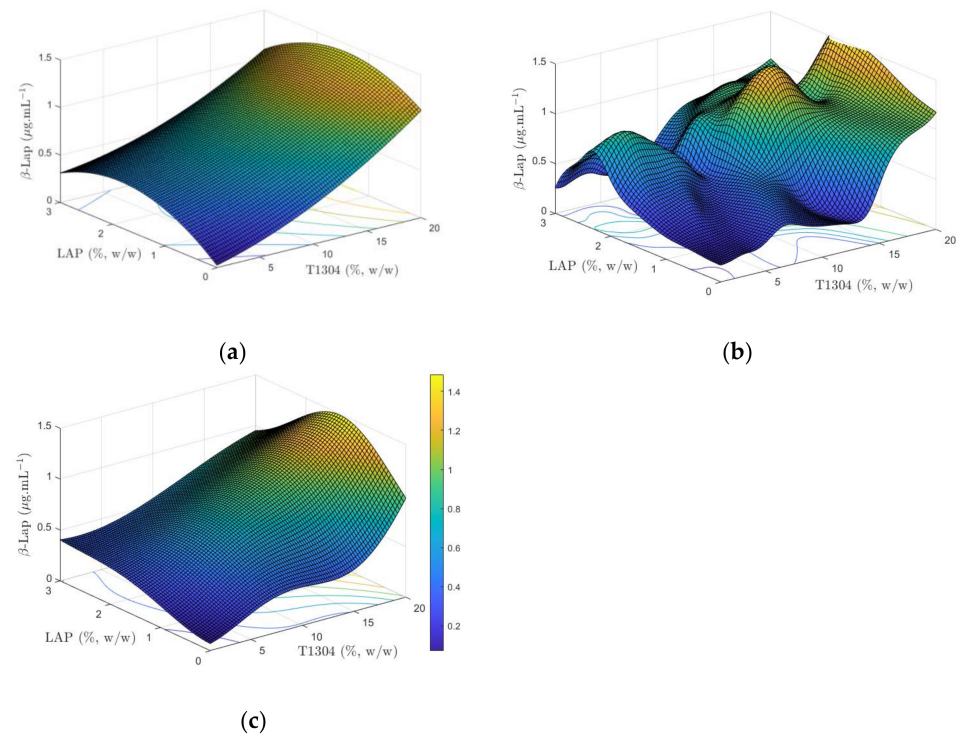


**Figure 7.** *β*-Lap solubility represented by response surface obtained by RSM (a), MLP (b), and SVM (c).

Table 4 presents the coefficients ( $\beta_{1-5}$ ) obtained from the RSM model and Table 5 presents the SVM-trained parameters.

**Table 4.** The coefficients ( $\beta_{1-5}$ ) obtained from the RSM model.

Parameters	Values	Parameters	Values
$\beta_0$	-0.0005	$\beta_{11}$	0.0015
$\beta_1$	0.0262	$\beta_{22}$	-0.1345
$\beta_2$	0.5031	$\beta_{12}$	-0.0057

**Table 5.** The parameters obtained from the SVM-trained model (bias = 0.8017).

Kernel Centers (or Support Vectors)	SVM Gains (See Figure 1b)
$c_1 = [1 \ 0.0]$	$\lambda_1 = 3.0335$
$c_2 = [5 \ 0.0]$	$\lambda_2 = -14.7519$
$c_3 = [5 \ 3.0]$	$\lambda_3 = -0.3119$
$c_4 = [10 \ 0.0]$	$\lambda_4 = 1.9719$
$c_5 = [10 \ 3.0]$	$\lambda_5 = -0.2327$
$c_6 = [15 \ 0.0]$	$\lambda_6 = -11.1711$
$c_7 = [15 \ 1.5]$	$\lambda_7 = 0.6484$
$c_8 = [20 \ 0.0]$	$\lambda_8 = 5.8914$
$c_9 = [20 \ 1.5]$	$\lambda_9 = 15$
$c_{10} = [20 \ 3.0]$	$\lambda_{10} = 1.8603$
$c_{11} = [20 \ 2.0]$	$\lambda_{11} = -10.1704$
$c_{12} = [8 \ 0.0]$	$\lambda_{12} = 15$
$c_{13} = [20 \ 1.0]$	$\lambda_{14} = -6.7674$

Table 6 shows the mean square error (MSE) and R-squared coefficient ( $R^2$ ) calculated from the resulting models of the RSM, MLP, and SVM. For the RSM, the MSE and  $R^2$  were calculated to the fitting values (assays 1–12 in Table 1) and validation values (assays 19–21 in Table 2). For MLP and SVM, the MSE and  $R^2$  were calculated to the training values (assays 1–9 in Table 1) and validation values (assays 19–21 in Table 2).

**Table 6.** Comparison between the techniques used.

Surface Method	MSE		$R^2$	
	Fitting	Val.	Fitting	Val.
RSM	0.0105	0.0109	0.9279	0.9368
	Training	Val.	Training	Val.
MLP	0.0106	0.0098	0.9332	0.9433
SVM	0.0030	0.0045	0.9814	0.9737

The results presented in Table 6 show that the ML based on the SVM had better results for the response surface than the other two techniques: MLP and RSM. The surface obtained based on the RSM strategy was limited by a mathematical expression of regression characterized by Equation (1), and this characteristic can limit the creation of the response surface, masking some characteristic behavior of the solution.

On the other hand, the MLP technique obtained measurements closer to the training points; although, in some regions, abrupt changes were found on the surface. It is essential to highlight that the success of the MLP is closely associated with the number of samples used in training. From an MSE perspective, the MLP and RSM presented similar results. However, the MLP technique showed better  $R^2$  results.

The surface found by the SVM technique had an expected behavior for the range of values used in the concentrations of T1304 ( $x_1$ ) and LAP ( $x_1$ ). Unlike the MLP technique,

there were no abrupt variations in the surface found by the SVM technique. In addition, SVM obtained a lower MSE value and a higher  $R^2$  value (see Table 6). Because of this, the SVM technique is presented as the best alternative for mounting the response surface.

#### 4. Conclusions

The hybrid and simple systems formed by different concentrations of T1304 with and without LAP presented different physical states when submitted to the temperature and pH ramp. It was observed that LAP significantly impacts the liquid–gel transition of the systems with the variations in temperature and pH. In addition, the solubility of  $\beta$ -Lap significantly increased, between 42–100-fold, depending on the compounds and concentrations of poloxamine and clay. The *in silico* study using ML and RSM computational tools showed fast and adequate strategies for predicting the phase behavior of nanocarrier systems; however, SVM promoted the finer adjustments of the data. The use of ML techniques can reduce the time of labor experimentation for the pre-formulation development of new nano-hybrid platforms. As proposals and future improvements, this work proposes using other machine learning techniques, such as Random Forest and k-nearest neighbors algorithm (kNN), to conduct a comparative analysis and attain better results than those presented in this manuscript.

**Author Contributions:** Data curation, C.C.L., F.F.d.O., C.V. and G.B.M.C.; methodology, F.F.d.O., R.d.M.B. and M.A.C.F.; project administration, M.A.C.F., E.B.S.; supervision, R.d.M.B.; writing—original draft, C.V., R.d.M.B. and M.A.C.F.; writing—review and editing, P.S., T.F.A.d.L.e.M., F.N.R., E.B.S. and M.A.C.F. All authors have read and agreed to the published version of the manuscript.

**Funding:** This research received no external funding.

**Institutional Review Board Statement:** Not applicable.

**Informed Consent Statement:** Not applicable.

**Data Availability Statement:** Not applicable.

**Acknowledgments:** We thank Celso Amorim Câmara from UFRPE for synthesizing  $\beta$ -Lap, BASF Corporation (Ludwigshafen, Germany), and BYK Additives & Instruments (Wesel, Germany) for donating Tetronic® 1304 and LAP, respectively, used in this work.

**Conflicts of Interest:** The authors declare no conflict of interest.

#### Abbreviations

PEO	poly (ethylene oxide)
PPO	poly (propylene oxide)
T1304	poloxamine with 21 and 27 PEO and PPO units respectively
LAP	Laponite
RMS	response surface methodology
ML	machine learning
MLP	multilayer perceptron
SVM	support vector machine
$\beta$ -Lap	$\beta$ -Lapachone
HBL	hydrophilic-lipophilic balance
SP1049C	doxorubicin
AI	artificial intelligence
ANN	artificial neural networks
SMO	sequential minimal optimization
CCD	central composite design
TPR	true positive rate
FNR	false negative rate
MSE	mean square error
kNN	k-nearest neighbors algorithm

## References

1. Úriz, A.; Sanmartín, C.; Plano, D.; Dreiss, C.A.; González-Gaitano, G. Activity Enhancement of Selective Antitumoral Selenodiazoles Formulated with Poloxamine Micelles. *Colloids Surf. B Biointerfaces* **2018**, *170*, 463–469. [[CrossRef](#)] [[PubMed](#)]
2. Nishiyama, N.; Kataoka, K. Current State, Achievements, and Future Prospects of Polymeric Micelles as Nanocarriers for Drug and Gene Delivery. *Pharmacol. Ther.* **2006**, *112*, 630–648. [[CrossRef](#)] [[PubMed](#)]
3. Oerlemans, C.; Bult, W.; Bos, M.; Storm, G.; Nijsen, J.F.W.; Hennink, W.E. Polymeric Micelles in Anticancer Therapy: Targeting, Imaging and Triggered Release. *Pharm. Res.* **2010**, *27*, 2569–2589. [[CrossRef](#)] [[PubMed](#)]
4. Tong, Y.C.; Chang, S.F.; Kao, W.W.Y.; Liu, C.Y.; Liaw, J. Polymeric Micelle Gene Delivery of Bcl-XL via Eye Drop Reduced Corneal Apoptosis following Epithelial Debridement. *J. Control. Release* **2010**, *147*, 76–83. [[CrossRef](#)]
5. Yokoyama, M. Clinical Applications of Polymeric Micelle Carrier Systems in Chemotherapy and Image Diagnosis of Solid Tumors. *J. Exp. Clin. Med.* **2011**, *3*, 151–158. [[CrossRef](#)]
6. Gong, J.; Chen, M.; Zheng, Y.; Wang, S.; Wang, Y. Polymeric Micelles Drug Delivery System in Oncology. *J. Control. Release* **2012**, *159*, 312–323. [[CrossRef](#)]
7. Zheng, C.; Zheng, M.; Gong, P.; Deng, J.; Yi, H.; Zhang, P.; Zhang, Y.; Liu, P.; Ma, Y.; Cai, L. Polypeptide Cationic Micelles Mediated Co-Delivery of Docetaxel and siRNA for Synergistic Tumor Therapy. *Biomaterials* **2013**, *34*, 3431–3438. [[CrossRef](#)]
8. Duncan, R.; Vicent, M.J. Polymer Therapeutics—Prospects for 21st Century: The End of the Beginning. *Adv. Drug Deliv. Rev.* **2013**, *65*, 60–70. [[CrossRef](#)]
9. Moghimi, S.M. Nanomedicine: Current Status and Future Prospects. *FASEB J.* **2005**, *19*, 311–330. [[CrossRef](#)]
10. Alvarez-Lorenzo, C.; Rey-Rico, A.; Sosnik, A.; Taboada, P.; Concheiro, A. Poloxamine-Based Nanomaterials for Drug Delivery. *Front. Biosci.* **2010**, *3*, 424–440. [[CrossRef](#)]
11. Alvarez-Lorenzo, C.; Sosnik, A.; Concheiro, A. PEO-PPO Block Copolymers for Passive Micellar Targeting and Overcoming Multidrug Resistance in Cancer Therapy. *Curr. Drug Targets* **2011**, *12*, 1112–1130. [[CrossRef](#)]
12. Schmolka, I.R. A Review of Block Polymer Surfactants. *J. Am. Oil Chem. Soc.* **1977**, *54*, 110–116. [[CrossRef](#)]
13. Alexandridis, P. Poly (Ethylene Oxide)/Poly (Propylene Oxide) Block Copolymer. *Curr. Opin. Colloid Interface Sci.* **1997**, *2*, 478–489. [[CrossRef](#)]
14. Inamdar, N.N.; Mourya, V. Applications of Polymers in Delivery of Biologics. In *Applications of Polymers in Drug Delivery*; Misra, A., Shahiwala, A., Eds.; Elsevier Inc.: Amsterdam, The Netherlands, 2021; pp. 449–534. [[CrossRef](#)]
15. Chiappetta, D.A.; Sosnik, A. Poly(Ethylene Oxide)-Poly(Propylene Oxide) Block Copolymer Micelles as Drug Delivery Agents: Improved Hydrosolubility, Stability and Bioavailability of Drugs. *Eur. J. Pharm. Biopharm.* **2007**, *66*, 303–317. [[CrossRef](#)]
16. Kuperkar, K.; Tiwari, S.; Bahadur, P. Self-Assembled Block Copolymer Nanoaggregates for Drug Delivery Applications. In *Applications of Polymers in Drug Delivery*; Misra, A., Shahiwala, A., Eds.; Elsevier Inc.: Amsterdam, The Netherlands, 2021; pp. 423–447. [[CrossRef](#)]
17. Tiwari, S.; Kansara, V.; Bahadur, P. Targeting Anticancer Drugs with Pluronic Aggregates: Recent Updates. *Int. J. Pharm.* **2020**, *586*, 119544. [[CrossRef](#)]
18. Rahdar, A.; Askari, F. Pluronic as Nano-Carrier Platform for Drug Delivery Systems. *Nanomed. Res. J.* **2018**, *3*, 174–179. [[CrossRef](#)]
19. Pillai, S.A.; Sharma, A.K.; Desai, S.M.; Sheth, U.; Bahadur, A.; Ray, D.; Aswal, V.K.; Kumar, S. Characterization and Application of Mixed Micellar Assemblies of PEO-PPO Star Block Copolymers for Solubilization of Hydrophobic Anticancer Drug and in Vitro Release. *J. Mol. Liq.* **2020**, *313*, 113543. [[CrossRef](#)]
20. Wolf, A.; Agnihotri, S.; Micallef, J.; Mukherjee, J.; Sabha, N.; Cairns, R.; Hawkins, C.; Guha, A. Hexokinase 2 Is a Key Mediator of Aerobic Glycolysis and Promotes Tumor Growth in Human Glioblastoma Multiforme. *J. Exp. Med.* **2011**, *208*, 313–326. [[CrossRef](#)]
21. Cuestas, M.L.; Sosnik, A.; Mathet, V.L. Poloxamines Display a Multiple Inhibitory Activity of ATP-Binding Cassette (ABC) Transporters in Cancer Cell Lines. *Mol. Pharm.* **2011**, *8*, 1152–1164. [[CrossRef](#)]
22. Cavalloro, G.; Fakhrullin, R.; Pasbakhsh, P. *Clay Nanoparticles: Properties and Applications*, 1st ed.; Cavalloro, G., Fakhrullin, R., Pasbakhsh, P., Eds.; Elsevier Inc.: Amsterdam, The Netherlands, 2020.
23. Tomás, H.; Alves, C.S.; Rodrigues, J. Laponite®: A Key Nanoplatfor for Biomedical Applications? *Nanomed. Nanotechnol. Biol. Med.* **2018**, *14*, 2407–2420. [[CrossRef](#)]
24. Ruzicka, B.; Zaccarelli, E. A Fresh Look at the Laponite Phase Diagram. *Soft Matter* **2011**, *7*, 1268–1286. [[CrossRef](#)]
25. Faustini, M.; Nicole, L.; Ruiz-Hitzky, E.; Sanchez, C. History of Organic-Inorganic Hybrid Materials: Prehistory, Art, Science, and Advanced Applications. *Adv. Funct. Mater.* **2018**, *28*, 1704158. [[CrossRef](#)]
26. Gaharwar, A.K.; Schexnailder, P.J.; Kline, B.P.; Schmidt, G. Assessment of Using Laponite? Cross-Linked Poly (Ethylene Oxide) for Controlled Cell Adhesion and Mineralization. *Acta Biomater.* **2011**, *7*, 568–577. [[CrossRef](#)]
27. Gonçalves, M.; Figueira, P.; Maciel, D.; Rodrigues, J.; Qu, X.; Liu, C.; Tomás, H.; Li, Y. PH-Sensitive Laponite®/Doxorubicin/Alginate Nanohybrids with Improved Anticancer Efficacy. *Acta Biomater.* **2014**, *10*, 300–307. [[CrossRef](#)]
28. Pelegrino, M.T.; de Araújo, D.R.; Seabra, A.B. S-Nitrosoglutathione-Containing Chitosan Nanoparticles Dispersed in Pluronic F-127 Hydrogel: Potential Uses in Topical Applications. *J. Drug Deliv. Sci. Technol.* **2018**, *43*, 211–220. [[CrossRef](#)]
29. Dos Santos, A.C.M.; Akkari, A.C.S.; Ferreira, I.R.S.; Maruyama, C.R.; Pascoli, M.; Guilherme, V.A.; de Paula, E.; Fraceto, L.F.; de Lima, R.; da Melo, P.S.; et al. Poloxamer-Based Binary Hydrogels for Delivering Tramadol Hydrochloride: Sol-Gel Transition Studies, Dissolution-Release Kinetics, in Vitro Toxicity, and Pharmacological Evaluation. *Int. J. Nanomed.* **2015**, *10*, 2391–2401. [[CrossRef](#)]

30. Barbosa, R.d.M.; Câmara, G.B.M.; García-Villén, F.; Viseras, C.; de Júnior, R.F.A.; Machado, P.R.L.; Câmara, C.A.; Farias, K.J.S.; de Moura, T.F.A.L.E.; Dreiss, C.A.; et al. Nanocomposite Gels of Poloxamine and Laponite for  $\beta$ -Lapachone Release in Anticancer Therapy. *Eur. J. Pharm. Sci.* **2021**, *163*, 105861. [[CrossRef](#)]
31. Silva, M.N.D.; Ferreira, V.F.; de Souza, M.C.B.V. Um Panorama Atual da Química e da Farmacologia de Naftoquinonas, Com Ênfase na Beta-Lapachona e Derivados. *Quim. Nova* **2003**, *26*, 407–416. [[CrossRef](#)]
32. Andrade-neto, V.F.D.; Goulart, O.F.; Silva, F.; Silva, J. Antimalarial Activity of Phenazines from Lapachol,  $\beta$ -Lapachone and Its Derivatives against *Plasmodium falciparum* in Vitro and *Plasmodium berghei* in Vivo. *Bioorg. Med. Chem. Lett.* **2004**, *14*, 1145–1149. [[CrossRef](#)] [[PubMed](#)]
33. Dos Santos, K.M.; de Melo Barbosa, R.; Vargas, F.G.A.; de Azevedo, E.P.; da Silva Lins, A.C.; Camara, C.A.; Aragão, C.F.S.; de Lima e Moura, T.F.; Raffin, F.N. Development of Solid Dispersions of  $\beta$ -Lapachone in PEG and PVP by Solvent Evaporation Method. *Drug Dev. Ind. Pharm.* **2018**, *44*, 750–756. [[CrossRef](#)] [[PubMed](#)]
34. Kim, I.; Kim, H.; Ro, J.; Jo, K.; Karki, S.; Khadka, P.; Yun, G.; Lee, J. Preclinical Pharmacokinetic Evaluation of  $\beta$ -Lapachone: Characteristics of Oral Bioavailability and First-Pass Metabolism in Rats. *Biomol. Ther.* **2015**, *23*, 296–300. [[CrossRef](#)]
35. Box, G.E.P.; Wilson, K.B. On the Experimental Attainment of Optimum Conditions. *J. R. Stat. Soc.* **1951**, *13*, 1–45. [[CrossRef](#)]
36. Singh, B.; Chakkal, S.K.; Ahuja, N. Formulation and Optimization of Controlled Release Mucoadhesive Tablets of Atenolol Using Response Surface Methodology. *AAPS PharmaSciTech* **2006**, *7*, E19–E28. [[CrossRef](#)]
37. Narayanan, H.; Dingfelder, F.; Butté, A.; Lorenzen, N.; Sokolov, M.; Arosio, P. Machine Learning for Biologics: Opportunities for Protein Engineering, Developability, and Formulation. *Trends Pharmacol. Sci.* **2021**, *42*, 151–165. [[CrossRef](#)]
38. McCoubrey, L.E.; Gaisford, S.; Orlu, M.; Basit, A.W. Predicting Drug-Microbiome Interactions with Machine Learning. *Biotechnol. Adv.* **2022**, *54*, 107797. [[CrossRef](#)]
39. De Souza, J.G.; Fernandes, M.A.C. A Novel Deep Neural Network Technique for Drug—Target Interaction. *Pharmaceutics* **2022**, *14*, 625. [[CrossRef](#)]
40. Bannigan, P.; Aldeghi, M.; Bao, Z.; Häse, F.; Aspuru-Guzik, A.; Allen, C. Machine Learning Directed Drug Formulation Development. *Adv. Drug Deliv. Rev.* **2021**, *175*, 113806. [[CrossRef](#)]
41. Hathout, R.M. Machine Learning Methods in Drug Delivery. In *Applications of Artificial Intelligence in Process Systems Engineering*; Ren, J., Shen, W., Man, Y., Dong, L., Eds.; Elsevier Inc.: Amsterdam, The Netherlands, 2021; pp. 361–380. [[CrossRef](#)]
42. Boulogeorgos, A.A.A.; Member, S.; Trevlakis, S.E.; Member, S.; Tegos, S.A.; Member, S.; Papanikolaou, V.K.; Member, S. Machine Learning in Nano-Scale Biomedical Engineering. *IEEE Trans. Mol. Biol. MULTI-SCALE Commun.* **2020**, *7*, 10–39. [[CrossRef](#)]
43. Shastry, K.; Sanjay, H. Machine Learning for Bioinformatics. In *Statistical Modelling and Machine Learning Principles for Bioinformatics Techniques*; Srinivasa, K.G., Siddesh, G.M., Manisekhar, S.R., Eds.; Springer: Singapore, 2020; pp. 25–39.
44. Naresh, E.; Kumar, B.; Shankar, S. Impact of Machine Learning in Bioinformatics Research. In *Statistical Modelling and Machine Learning Principles for Bioinformatics Techniques*; Srinivasa, K.G., Siddesh, G.M., Manisekhar, S.R., Eds.; Springer: Singapore, 2020; pp. 41–62.
45. Mouchlis, V.D.; Afantitis, A.; Serra, A.; Fratello, M.; Papadiamantis, A.G.; Aidinis, V.; Lynch, I.; Greco, D.; Melagraki, G. Advances in De Novo Drug Design: From Conventional to Machine Learning Methods. *Int. J. Mol. Sci.* **2021**, *22*, 1676. [[CrossRef](#)]
46. Boso, D.P.; Di Mascolo, D.; Santagiuliana, R.; Decuzzi, P.; Schrefler, B.A.; Morego, V. Drug Delivery: Experiments, Mathematical Modelling and Machine Learning. *Comput. Biol. Med.* **2021**, *123*, 103820. [[CrossRef](#)]
47. Pereira, A.K.V.; de Melo Barbosa, M.; Fernandes, M.A.C.; Finkler, L.; Finkler, C.L.L. Comparative Analyses of Response Surface Methodology and Artificial Neural Networks on Incorporating Tetracaine into Liposomes. *Braz. J. Pharm. Sci.* **2020**, *56*, e17808. [[CrossRef](#)]
48. Sun, Y.; Peng, Y.; Chen, Y.; Shukla, A.J. Application of Artificial Neural Networks in the Design of Controlled Release Drug Delivery Systems. *Adv. Drug Deliv. Rev.* **2003**, *55*, 1201–1215. [[CrossRef](#)]
49. Ekins, S.; Puhl, A.C.; Zorn, K.M.; Lane, T.R.; Russo, D.P.; Klein, J.J.; Hickey, A.J.; Clark, A.M. Exploiting Machine Learning for End-to-End Drug Discovery and Development. *Nat. Mater.* **2019**, *18*, 435–441. [[CrossRef](#)]
50. Bartolucci, R.; Magni, P. Application of Artificial Neural Networks to Predict the Intrinsic Solubility of Drug-Like Molecules. *Pharmaceutics* **2021**, *13*, 1101. [[CrossRef](#)]
51. Medarevi, D. Tailoring Atomoxetine Release Rate from DLP 3D-Printed Tablets Using Artificial Neural Networks: Influence of Tablet. *Molecules* **2021**, *26*, 111. [[CrossRef](#)]